pn-Junction Rectifiers Based on *p*-ZnO and *n*-ZnO Nanoparticles

Kallol Mohanta, Sudip K. Batabyal, and Amlan J. Pal*

Indian Association for the Cultivation of Science, Department of Solid State Physics and Centre for Advanced Materials, Kolkata 700032, India

Received January 27, 2007. Revised Manuscript Received March 29, 2007

We form *pn*-junctions by electrostatic binding of a *p*-type and an *n*-type ZnO nanoparticle. Current−voltage characteristics of *pn*-junctions are rectifying in nature. Individual components of the junction do not show any rectification. An *np*-junction, formed by reversing the binding sequence of the two types of nanoparticles, shows rectification in the reverse bias direction. By controlling the type of dopants in the ZnO nanoparticles, pn^+ (and n^+p) and nn^+ (and n^+n) junctions are formed that exhibit rectification. Current rectification in a junction between two nanoparticles shows that a depletion layer may have formed even in the quantum dot regime.

1. Introduction

Rectifying junctions are fundamental building blocks for basic electronics.[1−3] Hence, a junction between two nanostructures is of utmost importance for both nanoparticle and nanoelectronic research.[4−7] In this direction, ZnO can be considered as an ideal material because of its applications in electronic and opto-electronic devices.[8−10] Moreover, ZnO is one of the hardest materials in the family of II−VI semiconductors. While pristine ZnO nanoparticles with a wurtzite structure are a natural *n*-type semiconductor because of intrinsic defects, such as vacancies at the oxygen sites (V_O) and Zn interstitials (Zn_i),[11] they can be doped with Li during nanoparticle formation to obtain a *p*-type semiconductor.[12−14] Depending on the doping level, the nanoparticles offer many interesting electrical and optical properties.

The stabilizers with which growth of such nanoparticles are controlled can play a crucial role in assembling them on substrates. Functional groups of the stabilizers are key to such assemblies on suitably modified surfaces. One can select appropriate functional groups, so that the nanoparticles can be bound to the substrates via electrostatic absorption or layer-by-layer assembly.[15] The method of adsorption in such cases ensures that, at each stroke, only a monolayer of such particles gets deposited on the substrates. A repetition of the adsorption procedure with a polyion leads to multilayer films of nanoparticles for various applications.

The layer-by-layer deposition method may also allow assembly of two different types of materials[16] or particles in sequence. Such an assembly, between a *p*-type and an *n*-type nanoparticle, should lead to formation of a *pn*-junction. In this article, we present results on the formation of *pn*-junctions via electrostatic assembly of a *p*-type and an *n*-type nanoparticle as nanodiodes or rectifying nanocomposites.

2. Experimental Section

Materials. Mercaptoacetic acid ($HSCH_2COOH$), lithium chloride (LiCl), aluminum chloride ($AlCl_3$), poly(diallyldimethylammonium chloride) (PDDA), and chlorotrimethylsilane ($(CH_3)_3SiCl$) were purchased from Aldrich Chemical Co. Zinc acetate dihydrate, $(CH_3COO)_2Zn{\cdot}2H_2O$ (98%), hydrogen peroxide (H_2O_2), sodium hydroxide (NaOH), and ammonium hydroxide (NH_4OH) were purchased from E-Merck (India). All the chemicals were used without further purification. Deionized water (18.2 MΩ·cm) was obtained from a Milli-Q water purification system.

Substrates. Polished Si(111) wafers were arsenic doped (N-type) with a resistivity of 3−10 mΩ·cm. The wafers were cleaned in Piranha solution (3:1 mixture of H_2SO_4 acid and 30% H_2O_2) for 30 min followed by thorough rinsing in deionized water (**Warning:** Piranha solution reacts violently, even explosively, with organic materials. It should not be stored or combined with significant quantities of organic material.). Indium tin oxide (ITO) substrates

* Corresponding author. E-mail: sspajp@iacs.res.in.

(1) Metzger, R. M.; Chen, B.; Höpfner, U.; Lakshmikantham, M. V.; Vuillaume, D.; Kawai, T.; Wu, X.; Tachibana, H.; Hughes, T. V.; Sakurai, H.; Baldwin, J. W.; Hosch, C.; Cava, M. P.; Brehmer, L.; Ashwell, G. J. *J. Am. Chem. Soc.* **1997**, *119*, 10455.
(2) Lenfant, S.; Krzeminski, C.; Delerue, C.; Allan, G.; Vuillaume, D. *Nano Lett.* **2003**, *3*, 741.
(3) Wei, Z.; Kondratenko, M.; Dao, L. H.; Perepichka, D. F. *J. Am. Chem. Soc.* **2006**, *128*, 3134.
(4) Zhou, Y.; Gaur, A.; Hur, S. H.; Kocabas, C.; Meitl, M. A.; Shim, M.; Rogers, J. A. *Nano Lett.* **2004**, *4*, 2031.
(5) Harnack, O.; Pacholski, C.; Weller, H.; Yasuda, A.; Wessels, J. M. *Nano Lett.* **2003**, *3*, 1097.
(6) Gudiksen, M. S.; Lauhon, L. J.; Wang, J.; Smith, D. C.; Lieber, C. M. *Nature* **2002**, *415*, 617.
(7) Kovtyukhova, N. I.; Mallouk, T. E. *Adv. Mater.* **2005**, *17*, 187.
(8) Sun, B.; Sirringhaus, H. *Nano Lett.* **2005**, *5*, 2408.
(9) Zhu, Y.; Elim, H. I.; Foo, Y.-L.; Yu, T.; Liu, Y.; Ji, W.; Lee, J. -Y.; Shen, Z.; Wee, A. T. S.; Thong, J. T. L.; Sow, C. H. *Adv. Mater.* **2006**, *18*, 587.
(10) Verbakel, F.; Meskers, S. C. J.; Janssen, R. A. J. *Appl. Phys. Lett.* **2006**, *89*, 102103.
(11) Özgür, Ü.; Alivov, Y. I.; Liu, C.; Teke, A.; Reshchikov, M. A.; Doğan, S.; Avrutin, V.; Cho, S. J.; Morkoç, H. *J. Appl. Phys.* **2005**, *98*, 041301.
(12) Zeng, Y. J.; Ye, Z. Z.; Xu, W. Z.; Li, D. Y.; Lu, J. G.; Zhu, L. P.; Zhao, B. H. *Appl. Phys. Lett.* **2006**, *88*, 062107.
(13) Wang, X. H.; Yao, B.; Zhang, Z. Z.; Li. B. H.; Wei, Z. P.; Shen, D. Z.; Lu, Y. M.; Fan, X. W. *Semicond. Sci. Technol.* **2006**, *21*, 494.
(14) Lu, J. G.; Zhang, Y. Z.; Ye, Z. Z.; Zheng, Y. J.; He, H. P.; Zhu, L. P.; Huang, J. Y.; Wang, L.; Yuan, J.; Zhao, B. H.; Li, X. H. *Appl. Phys. Lett.* **2006**, *89*, 112113.
(15) Lee, D.; Rubner, M. F.; Cohen, R. E. *Nano Lett.* **2006**, *6*, 2305.
(16) Mukherjee, B.; Mohanta, K.; Pal, A. J. *Chem. Mater.* **2006**, *18*, 3302.

10.1021/cm070258p CCC: $37.00
Published on Web 06/30/2007

were cleaned sequentially by sonication in soap solution (1:10), distilled water (for several times), acetone, deionized water, methanol, and again in deionized water for 20, 10, 10, 10, 30, and 10 min, respectively. The Si and ITO substrates were protonated by dipping them in a mixture of isopropanol (98%, E-Merck, India) and chlorotrimethylsilane 10:1 (v/v) overnight. Some of the substrates were deprotonated in a mixture of H_2O, H_2O_2, and NH_4OH (5:2:2) for 1 h. Such substrates were used for adsorption of mercaptoacetic acid-capped and PDDA-capped ZnO nanoparticles.

Growth of Nanoparticles. To allow a natural junction formation, we stabilized the *p*- and *n*-type ZnO nanoparticles by an anionic and a cationic material, respectively. We used mercaptoacetic acid (MAA) and PDDA for this purpose. To obtain *n*-type ZnO nanoparticles (doping due to intrinsic defects), 40 mL of 4 mM solutions of zinc acetate and MAA each were mixed together and 0.2 mL of 1 N NaOH solution was added during vigorous stirring. The temperature was set to 60 °C. After 30 min, a transparent bluish-white solution resulted. To obtain *p*-type ZnO nanoparticles, 3.5 mg of LiCl was added before adding NaOH solution to the mixture of zinc acetate and MAA. To obtain *n*-type particles with higher doping concentration (n^+-type), 13.5 mg of $AlCl_3$ was added to the mixed solution during the growth. The nanoparticles were separated from the solution by centrifuging at 14 000 rpm for 30 min at 18 °C. They were redispersed in water for layer-by-layer (LbL) deposition. These solutions were anionic in nature due to the capping by mercaptoacetic acid. To make the nanoparticles cationic, 0.5 mL of an aqueous solution of PDDA (20 wt %) was added to 50 mL of mercaptoacetic acid-capped nanoparticles (0.02 wt %). After stirring for 30 min, the solution was centrifuged to isolate PDDA-capped nanoparticles. Again, they were dispersed in water for use as a cationic bath during LbL film deposition.

Formation of Rectifying Junctions. *pn*-Junctions were formed by sequential adsorption of *p*-type and *n*-type ZnO nanoparticles. To allow electrostatic adsorption between the particles, oppositely charged capping materials were chosen. That is, for a typical *pn*-junction, *p*-type particles with MAA capping were paired with an *n*-type one with PDDA. The sequence of particles was reversed to get an *np*-junction. Similarly, PDDA-capped *p*-type and MAA-capped *n*-type ZnO nanoparticles were paired to form *pn*- and *np*-junctions and exclude the effect of capping agents. In the same way, nn^+, n^+n, pn^+, and n^+p junctions (n^+ = Al-doped ZnO) were also formed. In all cases, sequential deposition of the two types of particles was carried out by dipping the substrates in suitable nanoparticle baths for 20 min. Because of surface charge reversal in LbL film deposition procedure, oriented junctions were formed on the substrates. The substrates were rinsed thoroughly after each monolayer deposition. The junctions were dried in vacuum at 80 °C for 2 h.

Characterization. UV−vis spectra of the nanoparticles were recorded with a HP5843 spectrometer by dispersing them in deionized water. Fourier transform infrared (FTIR) spectra were recorded with a Shimadzu 8300F spectrometer. A field emission scanning electron microscope (SEM, JEOL JSM-6700F) was used to examine surface morphology of the films. Individual nanoparticles and nanoparticle-junctions were characterized by a transmission electron microscope (TEM, JEOL JSM-2010). Crystalline structures of *n*-, *p*-, and n^+-type nanoparticles were examined by a Rich, Seifert XRD 3000P X-ray diffractometer with Cu Kα radiation (λ = 1.5418 Å). Atomic force microscope (AFM) images were recorded with a Veeco CPII AFM.

Monolayer of the junctions was kept in a vacuum chamber (1×10^{-3} Torr) at room temperature with the film facing downward. A syringe with a Hg blob on the tip of a metal needle was raised from outside the chamber slowly by a micrometer screw till the blob just touched the film. The diameter of the blob was <0.5 mm. The contact between the film and the blob was monitored through a microscope. Bias was applied with respect to the Hg electrode, and current−voltage ($I-V$) characteristics were recorded at both sweep directions and also in voltage loops. The $I-V$ characteristics were recorded with a Yokogawa 7651 dc source and a Keithley 486 picoammeter. The instruments were controlled by a personal computer via a general-purpose interface bus (GPIB). $I-V$ characteristics were also recorded with a Pt/Ir tip of a NanoSurf easyscan 2 scanning tunneling microscope (STM).

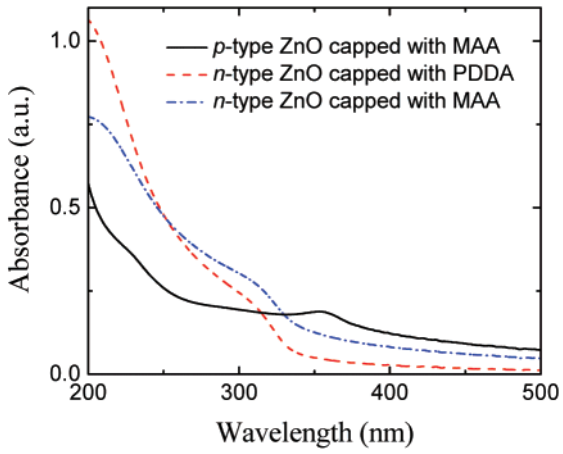

Figure 1. UV-Visible absorption spectra of the nanoparticles in dispersed solution.

3. Results and Discussion

Characterization of the Particles. We characterized the nanoparticles by X-ray diffraction (XRD),[17,18] electronic absorption, and infrared (IR) spectroscopy. XRD spectrum of *p*-, *n*-, and n^+-type nanoparticles show diffraction patterns corresponding to ZnO crystals. High-resolution transmission electron microscope (HRTEM) images of the particles show lattice spacing corresponding to ZnO crystals, confirming formation of ZnO crystals in the nanoparticles. IR spectra of the *p*- and *n*-type ZnO, capped with MAA and PDDA, respectively, show the presence of vibrations corresponding to the respective ligands in addition to Zn−O bending and stretching modes.[19,20] Absence of C═O vibrations in the former nanoparticles show that MAA was removed from the *p*-type nanoparticles. The spectra provide support to the thesis that PDDA capped the *n*-type nanoparticles through exchange reaction. UV−vis electronic absorption spectra of the *p*- and *n*-type particles in dispersed solution show peaks at 356 and 309 nm, respectively (Figure 1). For ZnO nanoparticles, the peak wavelengths correspond to particles with diameters of 3.2 and 1.6 nm, respectively (here, a band gap of 3.3 eV was considered for both particles[21]). Because of the change

(17) Andelman, T.; Gong, Y.; Polking, M.; Yin, M.; Kuskovsky, I.; Neumark, G.; O'Brien, S. *J. Phys. Chem. B* **2005**, *109*, 14314.
(18) Dhanajay; Nagaraju, J.; Roychaudhury, P.; Krupunidhi, S. B. *J. Phys. D: Appl. Phys.* **2006**, *39*, 2664.
(19) Wang, Z.; Zhang, H.; Wang, Z.; Zhang, L.; Yuan, J.; Yan, S.; Wang, C. *J. Mater. Res.* **2003**, *18*, 151.
(20) Colthup, N. B.; Daly, L. H.; Kimberley, S. E. *Introduction to Infrared and Raman Spectroscopy*; Academic Press: New York, 1964.
(21) Viswanatha, R.; Sapra, S.; Satpati, B.; Satyam, P. V.; Dev, B. N.; Sarma, D. D. *J. Mater. Chem.* **2004**, *4*, 661.

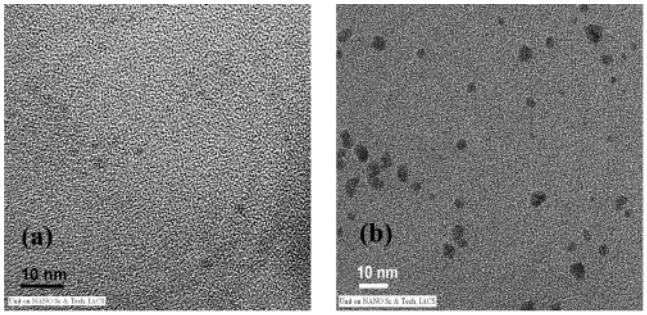

Figure 2. TEM images of (a) *n*-type and (b) *p*-type ZnO nanoparticles.

in capping, the spectra did not change, showing that the size remained unaltered during the exchange of the capping.

Images of the Nanoparticles (Morphological Characterization). AFM, SEM, and TEM images of the junctions and their components were recorded. AFM and SEM images exhibit that the surfaces were covered uniformly with nanoparticles. This is due to electrostatic adsorption of the capped-nanoparticles in LbL film deposition. Because of sequential adsorption of the nanoparticles, the directionality of the junctions is maintained over the area of the film.[15] TEM images of the *p*- and *n*-type nanoparticles, adsorbed on carbon-coated grids, show the individual particles (parts a and b of Figure 2). The pictures show that, when the particles were adsorbed on a substrate electrostatically, they did not form any clusters. Diameters of *p*- and *n*-type particles were ~3.5 and ~1.9 nm, respectively, which were below the quantum dot regime of ZnO. The values derived from the electronic absorption spectra[22] match reasonably well with the values obtained from the TEM images.

Rectifying Junctions. We have recorded $I-V$ characteristics of the junctions and the individual components by mercury probe and Pt/Ir tip of a STM. Films deposited on doped Si and ITO substrates were characterized. $I-V$ characteristics from a *pn*-junction are rectifying in nature (Figure 3a). An *np*-junction is also rectifying—with the $I-V$ characteristics being an inverse image to that of the *pn*-junction. The results characterizing a pair of nanoparticles in two opposite orientations between the same set of electrodes confirm that rectifying junctions between *p*- and *n*-type nanoparticles have formed. The rectifying characteristics are retraceable over many cycles and under different maximum voltage (V_{max}). Junctions on doped Si and ITO yielded rectification. $I-V$ characteristics from a number of *pn*-junctions (or *np*-junctions) are identical in nature, showing a high degree of reproducibility. Rectification in such junctions between the two nanoparticles must mean that a depletion layer formed between them. The ratio, which depends on the voltage at which it is measured, ranges between 3 and 7. The low value of rectification ratio may be due to long-chain polymer or heavy inert ion cappings on the nanoparticles reducing electric field at the depletion layer and consequent directional flow of carriers through it.

We have tried to fit the $I-V$ characteristics with the general empirical equation

$$I = I_0[\exp(eV/Nk_BT) - 1]$$

where I_0 is the reverse bias saturation current and k_B, T, and N are the Boltzmann's constant, temperature, and diode ideality factor, respectively. N determines the transport mechanism applicable in the rectifying diode. $N = 1$ corresponds to thermionic emission, while $N = 2$ leads to electron–hole recombination.[23,24] We have fitted the $I-V$ characteristics following the above equation and have obtained $N \approx 2.15$ at room temperature, which suggests that the transport through the junction may be due to electron–hole recombination.

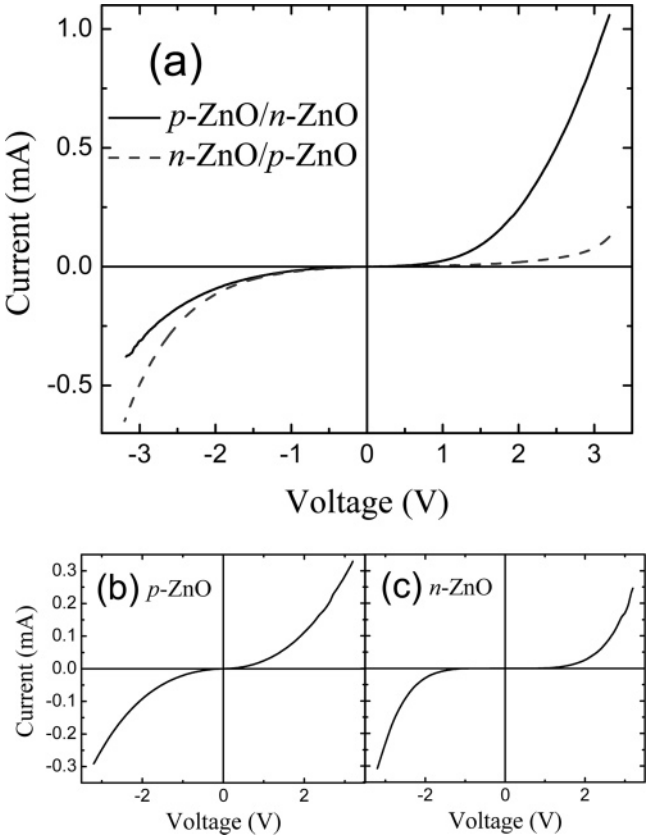

Figure 3. Current–voltage charateristics of (a) *pn*- and *np*-junctions based on assembly between a monolayer of MAA-capped *p*-type and a monolayer of PDDA-capped *n*-type ZnO nanoparticles. In (b) and (c), the characteristics for a monolayer of *p*-type and *n*-type nanoparticles, respectively, are shown. The junctions and the individual components were deposited on doped Si. Mercury was the other electrode.

Control Experiments. As control experiments, $I-V$ characteristics of the individual components of the junction, namely, *p*- and *n*-type ZnO nanoparticles, were recorded (parts b and c of Figures 3, respectively). Here also, we have characterized a number of particles and found a high degree of reproducibility. The characteristics of both *p*- and *n*-type nanoparticles under the identical experimental conditions (as for the *pn*- and *np*-junctions) show no trace of rectification. The symmetric $I-V$ characteristics are, however, nonlinear in both bias directions, representing nonohmic contact with the doped-Si and mercury electrodes.

The *pn*- and *np*-junctions, characterized by a STM tip, also show rectification (Figure 4a). Here also, the *np*-ones

(22) Pesika, N. S.; Stebe, K. J.; Searson, P. C. *Adv. Mater.* **2003**, *15*, 1289.
(23) Chai, Y.; Zhou, X.; Li, P. J.; Zhang, W.; Zhang, Q.; Wu, J. *Nanotechnology* **2005**, *16*, 2134.
(24) Streetman, B. G. *Solid-State Electronic Devices*; Prentice Hall: Englewood Cliffs, NJ, 1995.

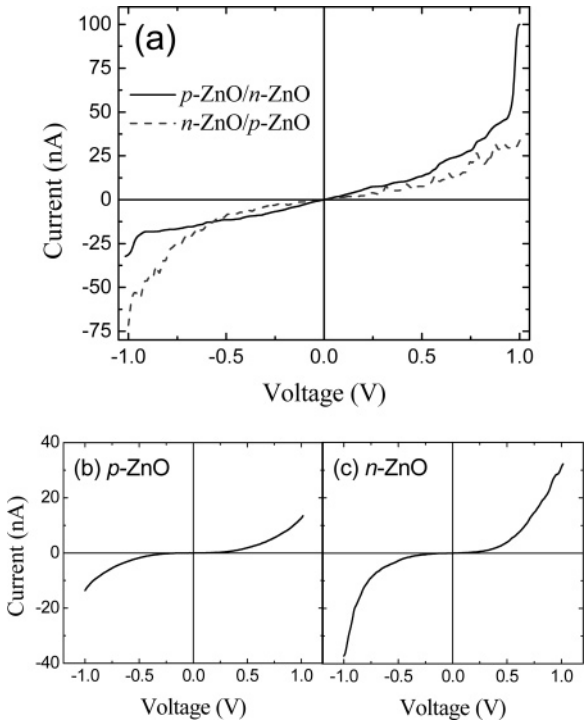

Figure 4. Current−voltage charateristics of (a) a *pn*- and an *np*-junction on doped-Si based on *p*-type and *n*-type ZnO nanoparticles with Pt/Ir tip of an STM. Characteristics of individual components are presented in (b) and (c), respectively.

exhibit rectification in the opposite direction as compared to the *pn*-junctions. The rectification ratios of the *pn*- and *np*-junctions match; they also match the values obtained with Hg as the other electrode. We have characterized monolayer of the individual nanoparticles with STM. Parts b and c of Figure 4 show $I-V$ plots for monolayers of *p*- and *n*-type ZnO nanoparticles, respectively. Here also, we have observed symmetric and nonohmic $I-V$ characteristics without any trace of rectifications. The results, hence, show that rectifying junctions were formed even in the microscopic scale.

As further control experiments, we studied the effect of the cappings, namely, MAA and PDDA in *p*- and *n*-type ZnO nanoparticles, respectively. To do so, we inversed the nature of stabilizers in the *p*- and *n*-type materials. That is, the *p*-type particles were capped with a cationic material (PDDA), while the *n*-type ones were capped with an anionic material (MAA). Both the *pn*- and *np*-junctions based on such nanoparticles were characterized (Figure 5). The $I-V$ characteristics show rectification similar to that presented in Figure 3a. Here also, the direction of rectification in *pn*-junction is opposite to that in *np*-one. The results show that the direction of current flow in the rectifying junctions depends only on the sequence between *p*- and *n*-type nanoparticles and *not* on the nature or junction between the capping layers. Junctions with only the stabilizers (PDDA/MAA or MAA/PDDA) also yield null results. Furthermore, a junction between two *n*-type nanoparticles with different stabilizers (*n*-ZnO capped with MAA and *n*-ZnO capped with PDDA) shows symmetric $I-V$ characteristics. We also have measured the $I-V$ with a direct contact between doped-Si and Hg. The $I-V$ due to 1−1.5

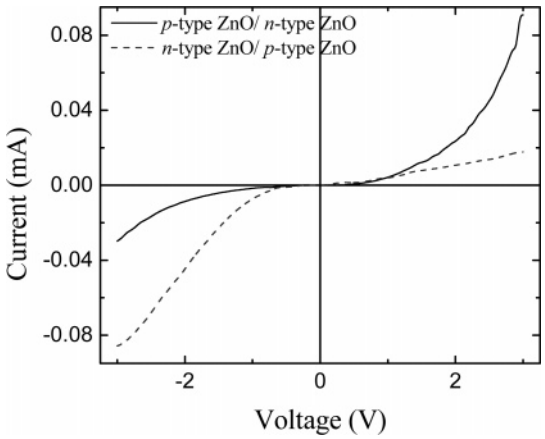

Figure 5. Current−voltage characteristics of a *pn*- and an *np*-junction between a monolayer of PDDA-capped *p*-type nanoparticles and a monolayer of MAA-capped *n*-type nanoparticles showing that rectification depends on the doping sequence in the two nanoparticles and *not* on capping materials.

nm native SiO_2 on Si was symmetric. Current with the nanoparticles was always less than that in the Si/Hg and MAA/PDDA (or PDDA/MAA) cases, evidencing the resistance offered by the nanoparticles.

Dopant Concentration Variation. To further validate formation of a rectifying junction between two nanoparticles, we introduced Al-doped n^+-type ZnO nanoparticles in the junctions. The current through a monolayer of n^+-ZnO nanoparticles is expectedly symmetric. At any voltage, it is higher as compared to that of *n*-ZnO nanoparticles. The higher current in n^+-ZnO is due to higher carrier concentration than in *n*-type nanoparticles. We used such n^+-type particles to form junctions with *n*- or *p*-type ones in the junctions. In effect, we formed n^+n and n^+p junctions. As reverse junctions, nn^+- and pn^+-junctions were also formed. Figure 6 shows $I-V$ characteristics of all the junctions that are rectifying in nature. Expectedly, the rectification ratio in n^+p- and pn^+-junctions is more than that in the *np*- and *pn*-cases. The ratio reaches up to 9.2. Here also, the rectification in a junction becomes reversed when its inverse junction is formed and characterized. For example, while an n^+p-junction shows rectification in the reverse bias, a pn^+-junction shows favorable current flow in the forward bias. The results, hence, confirm nanodiode or rectifying junction formation between two ZnO nanoparticles of different types/levels of dopants. The results obtained from *np* and *pn*, n^+p and pn^+, and n^+n and nn^+ junctions show that two nanoparticles with different levels of doping concentration form a rectifying junction. The current flow in all the junctions depends only on the sequence of doping levels in the two components.

4. Conclusion

In conclusion, we electrostatically bind two ZnO nanoparticles having different natures of doping. The two nanoparticles in effect form a *pn*-junction or a nanodiode. The junction exhibits electrical rectification demonstrating formation of a depletion layer between the two nanoparticles. While keeping the electrode combination the same, when

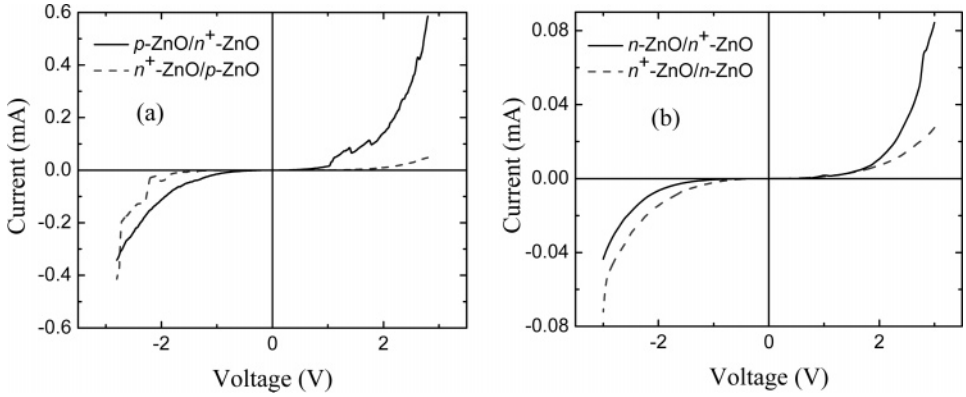

Figure 6. Current−voltage characteristics of (a) pn^+- and n^+p-junctions and (b) nn^+- and n^+n-junctions based on *p*-type, n^+-type, and *n*-type ZnO nanoparticles. The junctions were deposited on doped Si. Mercury was the other electrode.

junction formation is reversed, the direction of current rectification is also reversed. The rectification does not arise because of the cappings of the nanoparticles. The results obtained from *np* and *pn*, n^+p and pn^+, and n^+n and nn^+ junctions show that the current flow in junctions formed between two nanoparticles depends only on the sequence of doping levels in the two components. The results confirm nanodiode junction formation between a pair of nanoparticles.

Acknowledgment. K.M. acknowledges CSIR Junior Research Fellowship No. 9/80(491)/2005-EMR-I, Roll No. 509342). The Department of Science and Technology, Government of India, financially supported the work through Projects SP/S2/ M-44/99 and SR/S2/ RFCMP-02/2005.

Supporting Information Available: Characterization of *n*-, *p*-, and n^+-type nanoparticles (i.e., X-ray diffraction of different ZnO nanoparticles, IR spectra of MAA- and PDDA-capped ZnO nanoparticles, HRTEM image of the individual particles, AFM, SEM image of *pn*-junctions), $I-V$ characteristics of a number of *pn*-junctions ($I-V$ characteristics in loops, V_{max} dependence of a *pn*-junction, $I-V$ characteristics of *pn*-junctions at three different points), and some control experiments (i.e., theoretical fitting of typical $I-V$ characteristics of a *pn*-junction, comparison of $I-V$ characteristics of *n*-type and n^+-type ZnO nanoparticles) are shown as Supporting Information. This material is available free of charge via the Internet at http://pubs.acs.org.

CM070258P